

RD-UIE: Relation-Driven State Space Modeling for Underwater Image Enhancement

Kui Jiang
Harbin Institute of Technology
China

Yan Luo
Harbin Institute of Technology
China

Junjun Jiang
Harbin Institute of Technology
China

Xin Xu
Wuhan University of Science and
Technology
China

Fei Ma
Guangdong Laboratory of Artificial
Intelligence and Digital Economy (SZ)
China

Fei Yu
Shenzhen University
China

Abstract

Underwater image enhancement (UIE) is a critical preprocessing step for marine vision applications, where wavelength-dependent attenuation causes severe content degradation and color distortion. While recent state space models like Mamba show potential for long-range dependency modeling, their unfolding operations and fixed scan paths on 1D sequences fail to adapt to local object semantics and global relation modeling, limiting their efficacy in complex underwater environments. To address this, we enhance conventional Mamba with the sorting-based scanning mechanism that dynamically reorders scanning sequences based on statistical distribution of spatial correlation of all pixels. In this way, it encourages the network to prioritize the most informative components—structural and semantic features. Upon building this mechanism, we devise a Visually Self-adaptive State Block (VSSB) that harmonizes dynamic sorting of Mamba with input-dependent dynamic convolution, enabling coherent integration of global context and local relational cues. This exquisite design helps eliminate global focus bias, especially for widely distributed contents, which greatly weakens the statistical frequency. For robust feature extraction and refinement, we design a cross-feature bridge (CFB) to adaptively fuse multi-scale representations. These efforts compose the novel relation-driven Mamba framework for effective UIE (RD-UIE). Extensive experiments on underwater enhancement benchmarks demonstrate RD-UIE outperforms the state-of-the-art approach WMamba in both quantitative metrics and visual fidelity, averagely achieving 0.55 dB performance gain on the three benchmarks. Our code is available at <https://github.com/kkoucy/RD-UIE/tree/main>

Keywords

Underwater Image Enhancement, Mamba, Sorting

1 Introduction

Underwater image enhancement (UIE) improves the visual quality of degraded underwater scenes, serving as a critical pre-processing step for marine applications such as resource exploration, autonomous navigation, and biological monitoring.

Prior to deep learning technologies, conventional methods [1, 13, 17] employ hand-crafted priors for UIE, but struggle with generalization due to oversimplified assumptions. Deep learning methods [3, 7, 33] have advanced UIE performance, but still suffer from inherent limitations. For example, convolution Neural Networks (CNNs) are constrained by limited receptive fields. While Transformer-based

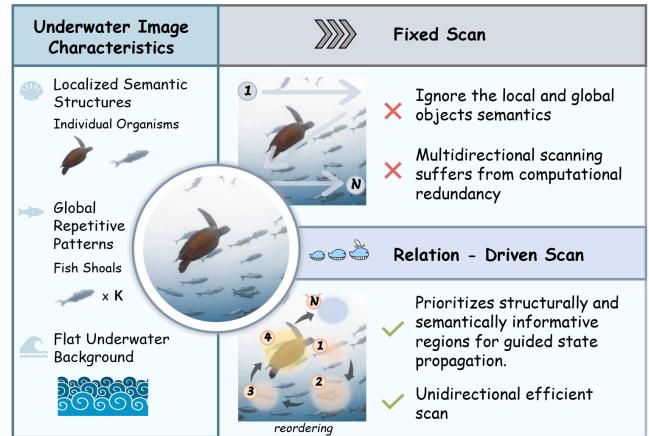


Figure 1: Underwater images contain localized semantic structures, global repetitive patterns and flat low-frequency backgrounds. While fixed scanning ignores these spatial heterogeneities, our relation-driven scan adaptively prioritizes structurally and semantically important regions, enabling efficient and context-aware state propagation.

architectures enhance feature representation through global modeling and effectively capture long-range dependencies, they incur substantial computational costs when processing high-resolution inputs. To balance global modeling with efficiency, recent works [8, 21] explore the Mamba architecture on State Space Models (SSMs), emerging as a promising alternative with linear complexity and robust global modeling capabilities.

Early Mamba-based adaptations for image restoration [18, 27, 38] employ rigid linear scanning patterns that propagate state information in fixed sequences. This approach inadequately explores semantic relationships and regionally significant features, limiting its capacity to simultaneously model (i) global contextual dependencies and (ii) localized structural semantics. As shown in Figure 1, underwater images exhibit two critical properties: i) local semantic structures (*e.g.*, individual marine organisms), and ii) global repetitive patterns (*e.g.*, fish shoals and coral reef arrangements). These observations suggest that robust feature representation necessitates the synergistic integration of broad contextual awareness and fine-grained structural cues. Recent advancements, such as multidirectional scanning strategies, aim to enhance spatial dependency

modeling. However, these methods introduce computational redundancy due to interference from irrelevant tokens [20], which can degrade modeling precision.

To address these limitations, we propose a relation-driven Mamba framework (RD-UIE) for underwater image enhancement. Our core insight is that updating a spatial location’s feature representation should prioritize aggregating contextual information from regions of semantic relevance or structural significance. Building on this principle, we design a dual-branch Visually Self-adaptive State Block (VSSB) comprising two key components: DS-Mamba and idConv. The former dynamically calculates sampling offset frequencies based on structural affinity and similarity, which inherently reflect the distribution of globally critical components. The input sequence is then reordered by these frequencies and processed via a unidirectional Mamba block, enabling priority-driven state propagation anchored to visually salient regions. The latter mitigates global focus bias by adaptively reshaping convolutional responses through dynamic kernel adjustments. This enhances local adaptability, particularly for low-frequency features (*e.g.*, homogeneous ocean backgrounds), which are frequent but lack discriminative detail. The dual-branch design is greatly compatible with the distinct characteristics of underwater scenes: ocean backgrounds exhibit large distribution areas but lower statistical frequency; marine organisms (*e.g.*, fish, corals) represent high statistical frequency and structurally semantic (validated quantitatively in Experiment 4.4). To further refine feature integration, we introduce a Cross-Feature Bridge (CFB) that adaptively fuses multi-scale representations through learnable channel-wise attention, ensuring robust hierarchical feature extraction. Collectively, these strategies underpin our novel RD-UIE approach, a relation-driven state space modeling for underwater image enhancement. The main contributions are summarized as follows.

- We propose a novel RD-UIE approach, where a relation-driven scanning mechanism is elaborated to dynamically reorder scanning sequences using activation frequency maps, improving modeling of spatially heterogeneous underwater structures.
- We design a hybrid enhancement architecture that combines dynamic sampling Mamba and dynamic convolution in a dual-branch mixer, augmented by CAB for spectral adaptation and CFB for cross-stage feature fusion.
- Our method achieves state-of-the-art performance on underwater enhancement benchmarks, with superior visual quality, generalization, and interpretability compared to existing methods.

2 Related Work

2.1 Underwater Image Enhancement

Existing underwater image enhancement (UIE) methods are broadly categorized into physics-based and learning-based approaches. Early model-driven techniques operate by estimating underwater optical parameters. For instance, UDCP [6] employs background light estimation and transmission refinement for color correction, while IBLA [26] incorporates a wavelength-dependent attenuation model.

However, these methods rely on idealized assumptions and frequently struggle in complex, non-uniform underwater environments. Learning-based methods, such as UWCNN, directly learn degraded-to-clear image mappings via CNNs but neglect underwater imaging priors, often yielding suboptimal color restoration. Two-stage frameworks like CLCE-Net [36] decouple color correction and deblurring but lack explicit physical constraints. Water-Net [16] introduces physical parameters but faces optimization instability due to tightly coupled parameter interactions.

2.2 Dynamic Convolution

While CNNs remain fundamental to image enhancement, their static convolutional kernels—with fixed sampling locations and weights—struggle to address the spatial heterogeneity of underwater degradation. Dynamic convolution mitigates this through two primary strategies. **Spatial-adaptive convolution:** Deformable Convolutional Networks (DCN) pioneer adaptive sampling through learned spatial offsets. Subsequent work like DAT [31] integrates attention mechanisms to improve spatial selectivity, though these methods retain fixed kernel weights. **Weight-adaptive convolution:** CondConv [34] introduces dynamic weight generation through conditional parameters, while DynamicConv [4] employs gated expert kernel selection. DyNet [37] enhances this approach with channel attention but incurs excessive parameters from full-channel modulation. To balance flexibility and efficiency, we introduce a "grouped dynamic convolution" that synthesizes content-aware kernel weights through channel-wise grouping and global pooling, aligning input dependencies with the Mamba branch to enable unified global-local modeling.

2.3 State Space Models

Mamba [8] represents a breakthrough in selective state space models (SSMs), introducing data-dependent state transitions with linear computational complexity. Its success in NLP has spurred adaptations to computer vision tasks, including 3D analysis, medical imaging, and low-level vision applications. Recent image restoration work demonstrates Mamba’s potential: MatIR [30] develops a hybrid Mamba–Transformer architecture with interleaved modules and multi-path SSM processing. FMSR [32] combines frequency-domain priors with Mamba for remote sensing enhancement, while Retinex-RAW-Mamba [2] integrates directional-Mamba scanning with Retinex decomposition for RAW image processing. Despite these advances, conventional Mamba architectures face two key limitations: 1) fixed scanning strategies struggle with spatially heterogeneous degradation patterns, and 2) insufficient consideration of local semantic relationships in feature aggregation. To address these challenges, we propose a relation-aware feature representation framework featuring a Visually Self-adaptive State Block (VSSB). Our VSSB enables the network to dynamically prioritize contextual information from semantically relevant or structurally critical regions through two key mechanisms: 1) frequency-based sequence reordering for scanning and 2) adaptively reshaping convolutional responses through dynamic kernel adjustment. This adaptive approach enhances feature representation quality while maintaining computational efficiency.

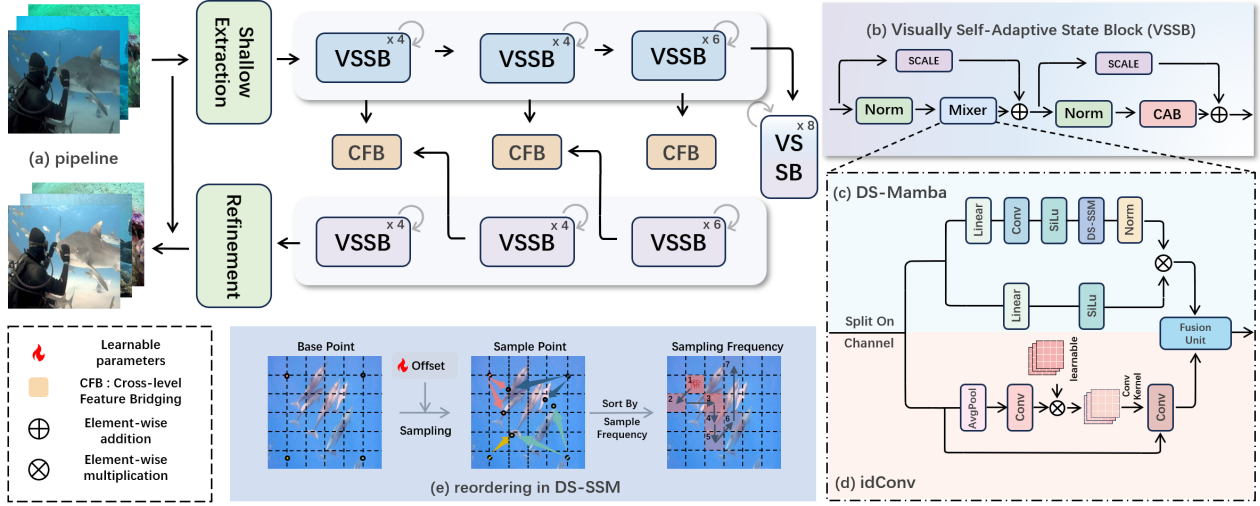


Figure 2: Overview of the proposed RD-UIE framework. (a) The overall pipeline follows an encoder-decoder architecture built upon stacked Visually Self-adaptive State Blocks. (b) Each VSSB adopts a Transformer-style residual layout with a Mixer–CAB structure. (c–d) Mixer: DS-Mamba performs relation-driven state propagation based on structurally informed sampling order, while idConv enhances local adaptability through input-dependent convolution. (e) Sampling and reordering in DS-SSM: calculating sampling offset frequencies and reordering based on structural affinity and similarity.

3 Methodology

Our enhancement framework is built upon a U-Net backbone and centers around a novel Visually Self-Adaptive State Block (VSSB), designed to address the spatial heterogeneity and wavelength-dependent color degradation observed in underwater imagery. As illustrated in Figure. 2, each VSSB contains a relation-driven dual-branch Mixer—consisting of DS-Mamba for global structure-aware modeling and idConv for local context adaptation alongside a channel modeling unit (CAB)[11] to address channel imbalance caused by differential light attenuation. In addition, we introduce a Cross-Feature Bridge (CFB) to bridge structural detail and semantic abstraction in encoder–decoder fusion. We detail each module in the following sections.

3.1 Visually Self-Adaptive State Block (VSSB)

As illustrated in Figure. 2(b), the Visually Self-adaptive State Block (VSSB) serves as the core computational unit in our framework. Each VSSB follows a Transformer-style residual design composed of a LayerNorm–Mixer–CAB stack with residual modulation, following the general structure of MambaIR [10].

To accommodate the dual distributions of underwater contents: spatially sparse but semantically critical foreground structures and statistically dominant low-frequency backgrounds, we adopt a dual-branch Mixer for spatial modeling. The first branch, DS-Mamba, introduces a relation-driven scanning mechanism that dynamically reorders the input sequence based on learned structural affinity, thereby prioritizing the modeling of globally significant regions such as object contours and repetitive textures. The second branch, idConv, complements this by adaptively refining convolutional responses in low-frequency areas, which typically lack high-frequency cues but occupy large spatial extents (e.g., open

water regions). This complementary design ensures that both detail-rich and texture-sparse areas receive adequate modeling capacity.

To further address channel bias, a lightweight channel modeling unit (CAB) is incorporated to recalibrate inter-channel dependencies, following the design principles in [10]. In general, VSSB achieves structurally aligned, content-aware enhancement by combining relation-driven propagation, local response adaptability, and mild color correction, enabling robust representation across diverse underwater conditions.

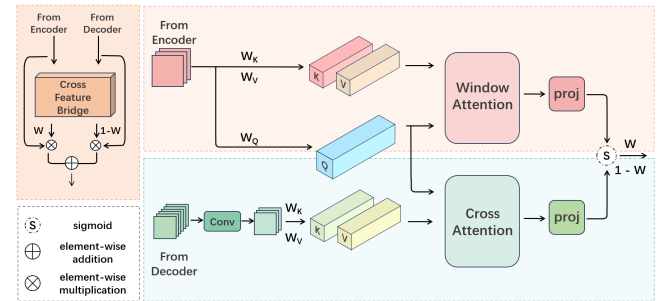


Figure 3: Illustration of the proposed Cross-Feature Bridge (CFB) module.

3.2 Mixer Module

The mixer module consists of two structurally complementary branches: DS-Mamba and idConv. We first divide the feature map $X \in \mathbb{R}^{H \times W \times C}$ along the channel into two parts notated as $X_1 \in \mathbb{R}^{H \times W \times C_1}$ and $X_2 \in \mathbb{R}^{H \times W \times C_2}$, where $C_1 = C_2 = \frac{C}{2}$. Then we feed X_1 and X_2 into DS-Mamba and idConv which are tailored to address different spatial characteristics in underwater imagery.

DS-Mamba (Dynamic Sampling Mamba). To address the fixed-order constraints inherent in conventional Mamba, we introduce DS-Mamba: a relation-driven variant that dynamically reorders the scanning sequence based on structural affinity. This approach aims to prioritize the propagation of states from regions that are structurally salient or exhibit strong feature continuity, a critical consideration for spatially heterogeneous underwater scenes.

At the core of DS-Mamba is a deformable sampling mechanism, inspired by deformable attention [31, 40]. Instead of relying on handcrafted saliency maps or fixed traversal schemes, we simulate deformable sampling by introducing a network of offsets. The offset generation network produces G groups of sampling offsets for each position p , with k^2 offsets per group, defined as:

$$\Delta_g^m(p) = f_{1 \times 1}(\text{GELU}(f_{\text{depth}}(X_1))) \begin{cases} m = 1, \dots, k^2 \\ g = 1, \dots, G \end{cases}, \quad (1)$$

where $X_1 \in \mathbb{R}^{H \times W \times C_1}$ is the input feature, f_{depth} refers to a 3×3 depthwise convolution, and $f_{1 \times 1}$ denotes a 1×1 convolution. The convolutional operation in the offset generation stage implicitly encodes local structural patterns, making the learned offsets responsive to nearby feature continuity and boundary transitions. This structural sensitivity underpins our sampling-based affinity estimation. Additionally, the group-wise strategy encourages specialization across different feature subsets, directing the sampling process toward context-rich structures such as edges, texture boundaries, and illumination transitions.

Each position p within each group generates new sampling locations using the computed offsets:

$$\hat{p}_g^m = p_{\text{base}} + \Delta_g^m(p), \quad (2)$$

where p_{base} represents the base position, and \hat{p}_g^m indicates the m^{th} sampling coordinate of position p in group g . Note that, for the generated non-integer sampling coordinates, we employ bilinear interpolation to compute the weighted values of the sampled locations, ensuring correct spatial transitions.

After obtaining \hat{p}_g^m , we calculate the sampling frequency for each position p within group g using the following equation:

$$\text{Cnt}_g(p) = \sum_{m=1}^{k^2} \mathbb{I}(p \in \hat{p}_g^m), \quad (3)$$

where $\mathbb{I}(\cdot)$ is the indicator function, which assigns a value of 1 if position p is sampled for the m^{th} time (i.e., $p \in \hat{p}_g^m$) and 0 otherwise.

Next, we partition the input feature map into G groups and sort the feature map $\{X_g\}_{g=1}^G$ according to $\text{Cnt}_g(p)$, resulting in a saliency-prioritized sequence $X_{\text{seq}} = \text{Sort}(X_g, \text{Cnt}_g(p))$. Finally, we use X_{seq} to feed the Mamba model for iterative updating of the hidden state:

$$h_t = Ah_{t-1} + BX_{\text{seq}}^t, \quad (4)$$

By initiating state transitions from these structurally salient anchors, DS-Mamba enables relation-driven propagation and long-range reasoning that aligns with the properties of underwater images, thereby improving both modeling accuracy and interpretability.

idConv (Input-dependent Convolution). To complement global modeling with localized adaptation, we introduce an input-dependent

dynamic convolution (idConv) branch. This module targets spatial regions that are statistically dominant yet often semantically sparse—such as homogeneous background water—where static kernels may fail to adaptively allocate modeling capacity.

Inspired by [22], idConv dynamically generates channel-specific convolutional kernels based on global context. Given an input feature map $X_2 \in \mathbb{R}^{H \times W \times C_2}$, we first apply global average pooling to extract channel-wise statistics. These are processed by two point-wise convolutions to compute group-wise attention weights:

$$\mathbf{A}' = \text{Conv}_{1 \times 1}^{\frac{C_2}{r} \rightarrow (G \times C_2)} \left(\text{Conv}_{1 \times 1}^{C \rightarrow \frac{C_2}{r}} (\text{AvgPool}(X_2)) \right), \quad (5)$$

$$\mathbf{A} = \text{Softmax}(\text{Reshape}(\mathbf{A}')), \quad (6)$$

$$\mathbf{W} = \sum_{i=1}^G \mathbf{P}_i \mathbf{A}_i, \quad (7)$$

where \mathbf{P}_i denotes the kernel bank for group i , and \mathbf{W} represents the final dynamic convolution weights. The resulting kernel \mathbf{W} varies across channels and is conditioned on the input distribution, enabling content-sensitive spatial responses.

To integrate the complementary features from DS-Mamba and idConv, we introduce a lightweight **FusionUnit**. The FusionUnit consists of a depthwise 3×3 convolution followed by two 1×1 convolutions with GELU activation and normalization. Let F_g and $F_l \in \mathbb{R}^{H \times W \times \frac{C}{2}}$ denote the outputs from the global (DS-Mamba) and local (idConv) branches, respectively. The fusion operator is depicted as:

$$F_{\text{out}} = \text{FusionUnit}(\llbracket F_g, F_l \rrbracket) + \llbracket F_g, F_l \rrbracket. \quad (8)$$

3.3 Cross-Feature Bridge (CFB)

To achieve more precise expression, we introduce a Cross-Feature Bridge (CFB) module that performs content-aware feature integration through dual-path attention and learnable channel-wise fusion, as shown in Figure. 3. Specifically, we treat encoder features as the structural source and decoder features as the semantic context, and design the fusion to account for their distinct roles.

Structural Encoder Attention. To preserve local detail and spatial fidelity, we apply local window self-attention to the encoder feature $F_h \in \mathbb{R}^{H \times W \times C}$:

$$\text{Attn}_h = \text{Softmax} \left(\frac{Q_h K_h^T}{\sqrt{d_k}} \right) V_h. \quad (9)$$

Semantic-guided Decoder Attention. To introduce global contextual cues from the decoder side $F_l' \in \mathbb{R}^{\frac{H}{2} \times \frac{W}{2} \times C}$, we perform asymmetric cross-attention using the encoder as a query:

$$\text{Attn}_l = \text{Softmax} \left(\frac{Q_h K_l^T}{\sqrt{d_k}} \right) V_l. \quad (10)$$

This allows the high-resolution encoder to selectively receive abstract guidance from deeper stages.

Channel-wise Gated Fusion. Instead of naive merging, we adopt a learnable channel attention gate to adaptively weigh the two

sources:

$$W = \text{sigmoid}(\text{Conv}_{1 \times 1}([\text{Attn}_h, \text{Attn}_l])), \quad (11)$$

$$F_{\text{out}} = W \odot F_h + (1 - W) \odot \text{Up}(F'_l). \quad (12)$$

Here, $W \in \mathbb{R}^{H \times W \times C}$ is a channel-spatial attention map that balances fine-grained structural detail with semantic abstraction.

3.4 Loss Functions and Constraints

Since underwater images typically exhibit both structural degradation and texture blur, we design a composite loss function that jointly optimizes pixel-wise fidelity, perceptual consistency, and edge preservation. The total loss consists of three components: ℓ_1 reconstruction loss, SSIM-based structure loss, and edge-aware loss.

Pixel-wise Loss. To ensure content-level consistency and suppress over-enhancement artifacts, we adopt the standard ℓ_1 loss:

$$L_{L1} = \frac{1}{N} \sum_{i=1}^N |\hat{y}_i - y_i|_1. \quad (13)$$

Structural Similarity Loss. We incorporate SSIM loss[29] to enhance the visual similarity in terms of luminance, contrast, and structural layout:

$$L_{\text{SSIM}} = 1 - \text{SSIM}(\hat{y}_i, y_i). \quad (14)$$

Edge Preservation Loss. To preserve high-frequency details and suppress structural blur, we use an edge-aware loss computed from Laplacian-based edge maps:

$$L_{\text{edge}} = \sqrt{(\text{Edges}(\hat{y}_i) - \text{Edges}(y_i))^2 + \epsilon^2}, \quad (15)$$

where $\text{Edges}(\cdot)$ denotes a fixed Laplacian edge extractor[15].

Total Objective. The final loss is a weighted sum:

$$L_{\text{total}} = \lambda_1 L_{L1} + \lambda_2 L_{\text{SSIM}} + \lambda_3 L_{\text{edge}}, \quad (16)$$

where we empirically set $\lambda_1 = 8$, $\lambda_2 = 1$, and $\lambda_3 = 4$ to balance pixel fidelity and structural preservation.

4 Experiments

4.1 Implementation Details

We conduct our experiments on two widely used real-world underwater image datasets: UIEB [16] and LSUI [25]. The UIEB dataset consists of 890 paired underwater images, where the reference image for each scene is selected via human voting by 50 volunteers from outputs generated by 12 enhancement algorithms. LSUI further extends scene diversity with 4,274 underwater images captured under varying lighting conditions, water types, and object categories. Reference images are selected from 18 algorithm outputs and finalized through ranking by 20 annotators.

For training, we randomly sample 830 paired images from UIEB and 3,300 from LSUI. All images are resized to a resolution of 256×256 . Our model is implemented in PyTorch 2.4.1 and trained on a single NVIDIA RTX 3090 GPU using the AdamW optimizer with an initial learning rate of 1×10^{-4} , and momentum parameters $(\beta_1, \beta_2) = (0.9, 0.999)$. The network is trained for 300,000 iterations with a batch size of 2, and a cosine annealing scheduler is employed for learning rate decay.

4.2 Experimental Settings

Benchmarks. We evaluate our method on both full-reference and no-reference underwater enhancement benchmarks. (1) *Full-reference test sets.* We use 60, 975, and 481 paired images from the UIEB, LSUI, and EUVP [14] datasets, denoted as TestU, TestL, and TestE, respectively. These datasets provide ground-truth references to assess pixel-level fidelity and structural accuracy. (2) *No-reference test sets.* To evaluate generalization on diverse underwater scenarios, we test on three unpaired benchmarks: 45 real-world images from U45 [19], 60 images from Challenge60[16], and 7 images from the Color-7 dataset, which focus on evaluating enhancement quality and color correction.

Compared Methods. We compare our method against six state-of-the-art underwater image enhancement (UIE) approaches: U-Trans [25], Semi-UIR [12], UIE-DM [28], CECF [5], HCLR-Net [39], and WMamba [9].

Evaluation Metrics. We adopt Peak Signal-to-Noise Ratio (PSNR), Structural Similarity Index (SSIM), and Mean Squared Error (MSE) for full-reference comparison, while the UCIQE [35], UIQM [24], and NIQE [23] are used as no-reference metrics. These metrics jointly assess underwater perceptual quality from contrast, color fidelity, naturalness, and sharpness perspectives.

4.3 Comparison with State-of-the-arts

We compare our method with six state-of-the-art underwater image enhancement methods on three full-reference benchmark subsets: TestU, TestL, and TestE. Table. 1 reports the quantitative results in terms of PSNR, SSIM, and MSE.

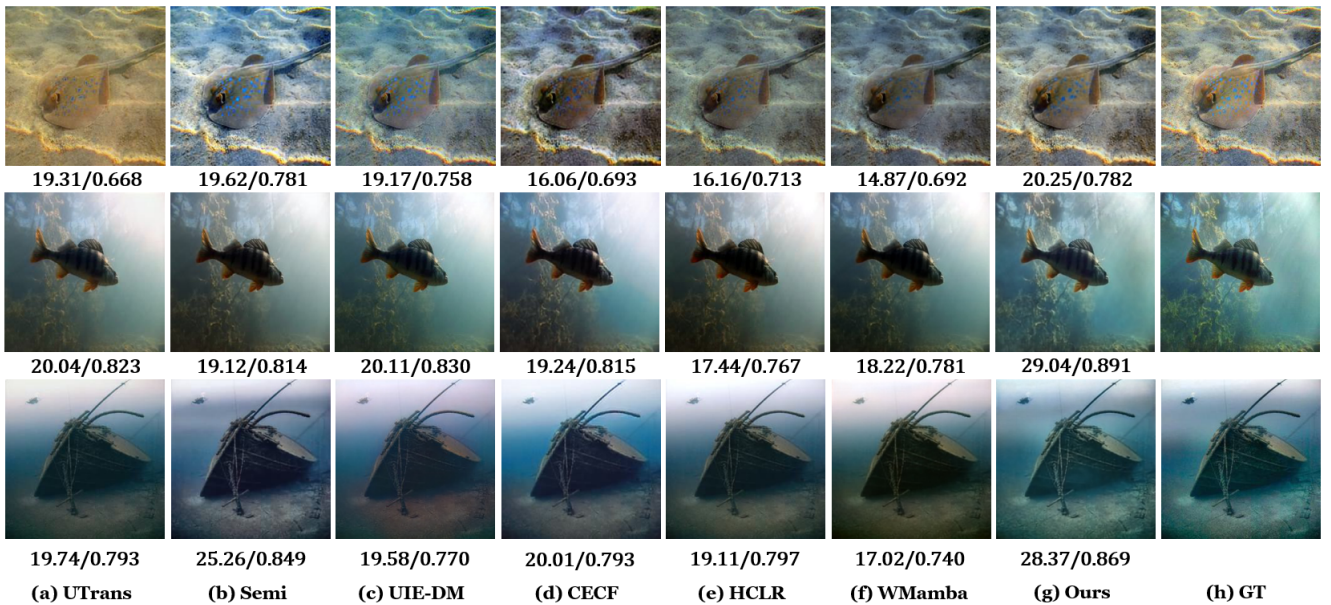
As shown in the Table. 1, our method consistently outperforms all competing approaches across all benchmarks. On TestU, our model achieves 24.91 dB PSNR, surpassing the previous best model [9] by 1.03 dB. On TestL, we attain a PSNR of 28.67 and the lowest MSE, highlighting superior structural restoration. On the most challenging TestE dataset, our approach reaches 29.09 PSNR and 0.896 SSIM, with significant margins over all baselines.

To further illustrate the effectiveness of our approach, Figure. 4 provides a visual comparison of three representative underwater scenes. U-Trans and Semi introduce obvious color deviation. For example, a noticeable yellow or blue shift in the first row leads to the appearance of an unnatural appearance in the whole figure or in the sand. CECF, HCLR, and WMamba struggle with enhancing the brightness and surface texture of the fish in the second row, resulting in a loss of detail. The recovery of the UIE-DM appears to be overcompensating for the red color and unnatural contents (the third row), especially in the water column. In contrast, our approach produces results with more substantial enhancement in detail, color, and illumination. We attribute these visible improvements to our proposed relation-driven scanning strategy and dual-branch representation design.

For a comprehensive evaluation, we compare our RD-UIE to other methods on three no-reference datasets: U45, C60, and Color7. The results are shown in Figure. 5 and Table. 2. Still, our RD-UIE is competitive, gaining the highest average scores in underwater-specific no-reference metrics—UCIQE and UIQM, with mean values of 0.603 and 3.079, respectively, across all three benchmarks. Figure. 5 presents visual comparisons, showing that the competitors

Table 1: Comparison of average PSNR/SSIM/MSE scores on TestU TestL and TestE datasets.

Method	TestU			TestL			TestE			Average Metrics		
	PSNR \uparrow	SSIM \uparrow	MSE \downarrow	PSNR \uparrow	SSIM \uparrow	MSE \downarrow	PSNR \uparrow	SSIM \uparrow	MSE \downarrow	PSNR \uparrow	SSIM \uparrow	MSE \downarrow
U-Trans [25]	20.77	0.801	92.17	24.23	0.842	80.57	25.33	0.823	74.59	23.44	0.822	82.44
Semi-UIR [12]	23.41	0.860	80.04	26.37	0.879	65.62	26.67	0.869	61.27	25.48	0.869	68.97
UIE-DM [28]	20.90	0.817	85.52	25.38	0.853	66.45	26.70	0.859	57.78	24.32	0.843	69.91
CECF [5]	21.52	0.815	87.28	23.73	0.839	79.65	23.26	0.813	79.70	22.83	0.822	82.21
HCLR [39]	23.72	0.861	77.15	27.44	0.877	58.01	27.69	0.857	53.13	26.28	0.864	62.76
WMamba [9]	23.88	0.865	77.05	28.33	0.889	52.26	28.76	0.881	45.50	26.99	0.878	58.27
Ours	24.91	0.891	74.16	28.67	0.911	51.07	29.09	0.896	45.40	27.54	0.897	56.87

**Figure 4: Restoration results of different methods for different degradation types. (a) UTrans[25] , (b) Semi[12] , (c) UIE-DM[28] , (d) CECF[5] , (e) HCLR[39] , (f) WMamba[9] , (g) Ours , and (h) Ground Truth.**

(such as UIE-DM, CECF and HCLR) produce unsatisfactory enhanced results with artifacts and color distortion. While WMamba enhances the texture representation, it does not cope well with the blue and green bias of the first scenario of raw underwater images. In contrast, our method maintains more natural contrast and texture across a variety of degradation types, demonstrating better generalization and robustness under diverse underwater imaging conditions.

4.4 Analysis of Stage-Aware Dynamic Sampling

To gain further insight into how our relation-driven sampling mechanism adapts to spatial context, we visualize the learned activation frequency maps from both the encoder and decoder stages.

Encoder Sampling Reflects Structural Importance. As shown in Figure. 6, the encoder-stage sampling maps exhibit a strong correlation with semantically and structurally meaningful regions across a variety of underwater scenes. This behavior is not manually designed, but emerges implicitly from our model’s offset learning mechanism. Specifically, the deformable sampling offsets are generated by a lightweight CNN that captures local structural continuity

and texture contrast—features that are commonly aligned with object boundaries and semantic saliency.

In the first row, the encoder concentrates its sampling on the contours of the school of fish. These regions present repetitive edge-like textures that are globally distributed, and thus provide rich structural anchors for propagation. In the second row, the model prioritizes the arms of the starfish as well as similarly colored stones in the background, suggesting that the offset generator is sensitive to both local contrast and color affinity, which together contribute to semantic relevance. In the third row, the sampling frequencies peak at the bright ridges of coral tips, where illumination transitions sharply, demonstrating the model’s ability to detect fine-grained, high-frequency edges likely to indicate meaningful boundaries.

These patterns indicate that our model does not sample based on fixed spatial priors or intensity peaks alone. Rather, the learned offsets adaptively direct attention to regions exhibiting relational cues—such as boundary sharpness, texture discontinuities, or semantic resemblance—thereby enabling relation-driven state propagation. This capacity to learn what regions matter most, without

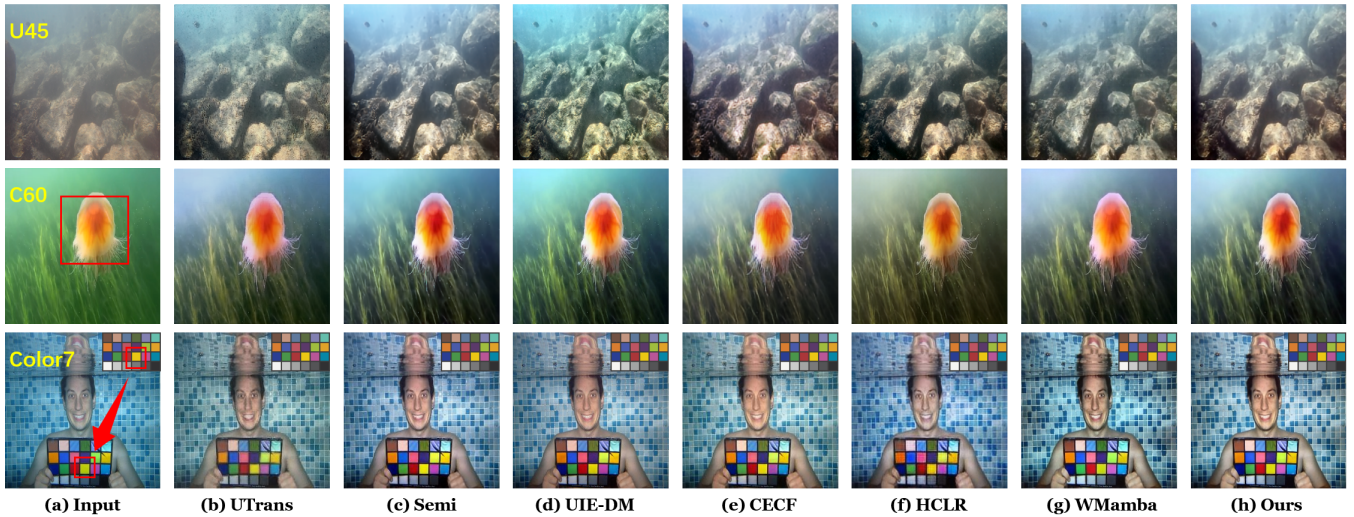


Figure 5: Visual comparisons results on the real-world U45/C60/Color7 datasets. (b) U-Trans[25], (c) Semi[12], (d) UIE-DM[28], (e) CECF[5], (f) HCLR[39], (g) WMamba[9], (h) Ours

Table 2: Quantitative comparisons on four no-reference test sets using UCIQE, UIQM, and NIQE metrics. Higher UCIQE and UIQM scores indicate better contrast, colorfulness, and Lower Niqe means a more natural visual effect. In the table, the best result is in bold, the second is underlined, and the third is dotted line.

Datasets	Metrics	UTrans[25]	Semi[12]	UIE-DM[28]	CECF [5]	HCLR[39]	WMamba [9]	Ours
U45	UCIQE \uparrow	0.567	0.605	<u>0.603</u>	0.592	0.591	0.596	<u>0.600</u>
	UIQM \uparrow	3.105	<u>3.130</u>	<u>3.107</u>	3.101	3.168	3.063	3.102
	NIQE \downarrow	4.664	5.346	4.100	5.814	<u>4.637</u>	<u>4.627</u>	4.892
C60	UCIQE \uparrow	0.545	0.585	0.579	<u>0.582</u>	0.565	0.576	<u>0.581</u>
	UIQM \uparrow	2.659	2.648	2.577	<u>2.724</u>	2.737	2.659	<u>2.676</u>
	NIQE \downarrow	6.295	7.849	7.359	7.247	6.648	<u>6.535</u>	<u>6.645</u>
Color7	UCIQE \uparrow	0.564	0.619	0.606	0.603	<u>0.614</u>	0.628	<u>0.627</u>
	UIQM \uparrow	3.463	3.219	<u>3.385</u>	3.300	3.274	<u>3.344</u>	3.460
	NIQE \downarrow	4.670	4.814	5.096	5.031	<u>4.799</u>	4.859	<u>4.704</u>
Average Metric	UCIQE \uparrow	0.558	0.603	0.596	0.592	0.590	<u>0.600</u>	0.603
	UIQM \uparrow	<u>3.075</u>	2.999	3.023	3.041	<u>3.059</u>	3.022	3.079
	NIQE \downarrow	5.209	6.003	5.518	6.030	<u>5.243</u>	<u>5.340</u>	5.347

explicit supervision, validates our motivation of building a structure-aware and semantically informed encoder.

Decoder Sampling Reflects Semantic Convergence. In the decoder stage, we observe a shift toward more uniformly distributed sampling frequencies across spatial locations. Rather than contradicting our relation-driven design, this behavior reflects the decoder’s distinct functional role: consolidating encoded structural cues into coherent, high-level representations. While encoder sampling aggressively targets salient structures for relation-driven propagation, decoder sampling favors broader contextual integration to ensure spatial consistency and visual coherence.

Notably, sampling in the decoder still exhibits alignment with major semantic boundaries (e.g., object contours), albeit in a less concentrated fashion. This supports the notion that decoder refinement benefits from structurally-aware encoding but does not

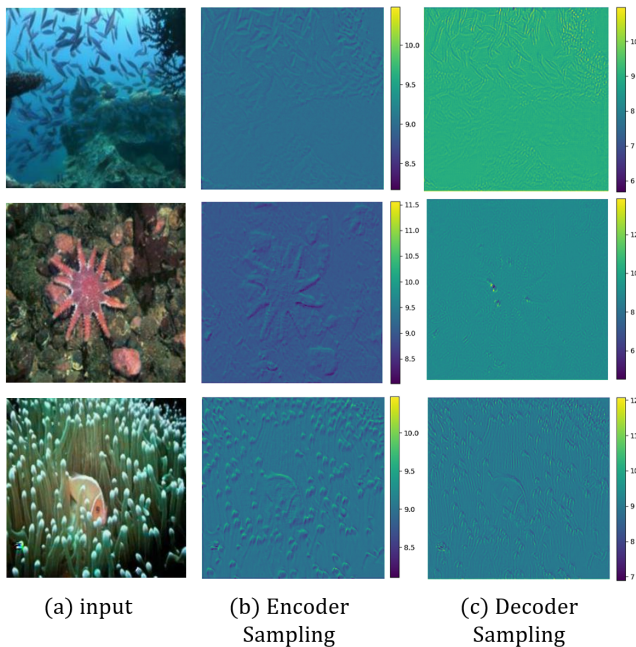
require repeated emphasis on the same localized features. These complementary behaviors underscore the flexibility of our proposed dynamic scanning mechanism.

4.5 Ablation Study

Effects of Sampling Hyperparameter k . We observe a non-monotonic trend where performance first improves and then slightly drops as k increases. We hypothesize that larger k increases the sampling diversity, allowing the model to explore more potential structural patterns. However, overly large k may introduce redundant or noisy offsets, diluting the importance of salient features and thus hindering convergence. Related results are shown in Table 3. Finally, we choose 3 as the sampling hyperparameter in our network.

Table 3: Ablation on sampling size k and scan strategies.

Variant Name	PSNR \uparrow	SSIM \uparrow
Sampling $k = 1$	28.48	0.883
Sampling $k = 2$	28.58	0.894
Sampling $k = 3$	28.67	0.911
Sampling $k = 4$	28.67	0.909
Sampling $k = 5$	28.59	0.908
Normal four-direction scan	28.52	0.905
Two-direction scan (ours + bidir)	28.47	0.908
Ours (single-direction scan)	28.67	0.911

**Figure 6: Visualization of sampling frequency maps in encoder and decoder stages.**

Effects on scan method. We conduct two experiments to evaluate the effectiveness of our proposed scan strategy.

First, we replace our directional scan with a traditional four-directional sequential scan, which leads to a performance drop. This indicates that our scan design better captures spatial dependencies and context adaptivity.

Second, we maintain the scanning order but reverse the information flow from a unidirectional propagation to a bidirectional design. Interestingly, this modification leads to a noticeable drop in performance. We attribute this to the disruption of relation-driven consistency: our original one-way design ensures that structurally salient regions propagate first, offering relational guidance to less informative areas. In contrast, the reversed flow allows low-relevance or noisy regions to influence high-confidence areas, potentially introducing structural ambiguity and semantic noise. This result reinforces the importance of prioritizing relation-rich regions in a directional manner, aligning with our core design philosophy.

Effects of Architectural Components. To evaluate the effectiveness of each architectural component, we conduct ablation studies

Table 4: Comparison of Different Configurations in Our Architecture.

Model Variant	Freq. Scan	idConv	CFB	PSNR \uparrow	SSIM \uparrow
(a) only Mamba	✓	✗	✗	28.38	0.894
(b) only idConv	✗	✓	✗	28.05	0.897
(c) only Mixer	✓	✓	✗	28.39	0.895
(d) Mixer + CFB (full)	✓	✓	✓	28.67	0.911
(e) idConv \rightarrow 3x3Conv	✓	✗	✓	28.51	0.895

by selectively removing or altering individual modules, as shown in Table. 4.

We first analyze the impact of our dual-branch Mixer. Variant (a), which uses only the frequency-sorted DS-Mamba, and variant (b), which uses only idConv, both perform poorly compared to the full Mixer in (c), confirming their complementary nature. In particular, although (a) and (c) exhibit similar PSNR scores, the introduction of idConv reduces FLOPs by nearly half. This highlights idConv’s practical value in deployment-constrained scenarios. It is worth noting that in variant (a/b/c), jump connections use the most common pattern of element-wise addition. Thus, the comparison Model of (c) and (d) can illustrate the effectiveness of our CFB module. When CFB is further introduced in variant (d) to form a complete network, we observe the best SSIM of 0.911, validating the importance of hierarchical attention-based fusion in preserving structure-semantic consistency across encoder-decoder stages. Replacing idConv with a static 3×3 convolution in (e) results in a performance drop, emphasizing the value of its input-adaptive formulation. These results collectively demonstrate that the synergistic design of dynamic global scanning, efficient local refinement, and cross-stage feature fusion is crucial for achieving both performance and efficiency in our RD-UIE framework.

5 Conclusion

In this paper, we present RD-UIE, a Relation-Driven State Space Modeling framework for underwater image enhancement. Targeting the structural and semantic complexities of underwater scenes, RD-UIE introduces a dynamic scanning mechanism that prioritizes state propagation from globally critical regions. The proposed framework is built upon three key components: (1) DS-Mamba: A relation-aware component that employs deformable sampling offsets to dynamically reorder input sequences based on structural affinity, enabling adaptive global feature modeling. (2) idConv: An input-adaptive convolutional layer for local refinement, complementing global modeling by resolving fine-grained distortions. (3) Cross-Feature Bridge (CFB): A dual-path attention module that integrates hierarchical features while preserving spatial and semantic relationships. Extensive experiments on synthetic and real-world benchmarks demonstrate RD-UIE’s state-of-the-art performance. Our framework outperforms existing methods by 1.03 dB in PSNR, achieving superior visual consistency and interpretability. Ablation studies and feature visualizations validate the efficacy of our dynamic sampling strategy and dual-branch architecture.

References

- [1] Cosmin Ancuti, Codruta Ormiana Ancuti, Tom Haber, and Philippe Bekaert. 2012. Enhancing underwater images and videos by fusion. In *2012 IEEE Conference on Computer Vision and Pattern Recognition*. 81–88.
- [2] Xianmin Chen, Peiliang Huang, Xiaoxu Feng, Dingwen Zhang, Longfei Han, and Junwei Han. 2024. Retinex-RAWMamba: Bridging Demosaicing and Denoising for Low-Light RAW Image Enhancement. *ArXiv abs/2409.07040* (2024).
- [3] Xuelei Chen, Pin Zhang, Lingwei Quan, Chao Yi, and Cunyu Lu. 2021. Underwater Image Enhancement based on Deep Learning and Image Formation Model. *arXiv:2101.00991*
- [4] Yinpeng Chen, Xiyang Dai, Mengchen Liu, Dongdong Chen, Lu Yuan, and Zicheng Liu. 2020. Dynamic convolution: Attention over convolution kernels. In *Proceedings of the IEEE/CVF conference on computer vision and pattern recognition*. 11030–11039.
- [5] Xiaofeng Cong, Jie Gui, and Junming Hou. 2024. Underwater Organism Color Fine-Tuning via Decomposition and Guidance. In *AAAI Conference on Artificial Intelligence*.
- [6] P. Drews Jr, E. do Nascimento, F. Moraes, S. Botelho, and M. Campos. 2013. Transmission Estimation in Underwater Single Images. In *2013 IEEE International Conference on Computer Vision Workshops*. 825–830.
- [7] Zhenqi Fu, Xiaopeng Lin, Wu Wang, Yue Huang, and Xinghao Ding. 2022. Underwater Image Enhancement Via Learning Water Type Desensitized Representations. In *ICASSP 2022 - 2022 IEEE International Conference on Acoustics, Speech and Signal Processing (ICASSP)*. 2764–2768.
- [8] Albert Gu and Tri Dao. 2023. Mamba: Linear-Time Sequence Modeling with Selective State Spaces. *ArXiv abs/2312.00752* (2023).
- [9] Meisheng Guan, Haiyong Xu, Gangyi Jiang, Mei Yu, Yeyao Chen, Ting Luo, and Yang Song. 2024. WaterMamba: Visual State Space Model for Underwater Image Enhancement. *ArXiv abs/2405.08419* (2024).
- [10] Hang Guo, Jinmin Li, Tao Dai, Zhihao Ouyang, Xudong Ren, and Shu-Tao Xia. 2024. MambaLR: A Simple Baseline for Image Restoration with State-Space Model. *arXiv:2402.15648 [cs.CV]*
- [11] Jie Hu, Li Shen, and Gang Sun. 2018. Squeeze-and-Excitation Networks. In *2018 IEEE/CVF Conference on Computer Vision and Pattern Recognition*. 7132–7141.
- [12] Shirui Huang, Keyan Wang, Huan Liu, Jun Chen, and Yunsong Li. 2023. Contrastive Semi-Supervised Learning for Underwater Image Restoration via Reliable Bank. *2023 IEEE/CVF Conference on Computer Vision and Pattern Recognition (CVPR)* (2023), 18145–18155.
- [13] Kashif Iqbal, Michael Odetayo, Anne James, Rosalina Abdul Salam, and Abdullah Zawawi HJ Talib. 2010. Enhancing the low quality images using Unsupervised Colour Correction Method. In *2010 IEEE International Conference on Systems, Man and Cybernetics*. 1703–1709.
- [14] Md Jahidul Islam, Youya Xia, and Junaed Sattar. 2020. Fast Underwater Image Enhancement for Improved Visual Perception. *IEEE Robotics and Automation Letters* 5, 2 (2020), 3227–3234.
- [15] Wei-Sheng Lai, Jia-Bin Huang, Narendra Ahuja, and Ming-Hsuan Yang. 2017. Deep Laplacian Pyramid Networks for Fast and Accurate Super-Resolution. In *2017 IEEE Conference on Computer Vision and Pattern Recognition (CVPR)*. 5835–5843.
- [16] Chongyi Li, Chunle Guo, Wenqi Ren, Runmin Cong, Junhui Hou, Sam Kwong, and Dacheng Tao. 2020. An Underwater Image Enhancement Benchmark Dataset and Beyond. *IEEE Transactions on Image Processing* 29 (2020), 4376–4389.
- [17] Chong-Yi Li, Ji-Chang Guo, Run-Min Cong, Yan-Wei Pang, and Bo Wang. 2016. Underwater Image Enhancement by Dehazing With Minimum Information Loss and Histogram Distribution Prior. *IEEE Transactions on Image Processing* 25, 12 (2016), 5664–5677.
- [18] Dong Li, Yidi Liu, Xueyang Fu, Senyan Xu, and Zheng-Jun Zha. 2024. FourierMamba: Fourier Learning Integration with State Space Models for Image Deraining. *arXiv preprint arXiv:2405.19450* (2024).
- [19] Hanyu Li, Jingjing Li, and Wei Wang. 2019. A Fusion Adversarial Underwater Image Enhancement Network with a Public Test Dataset. *arXiv:1906.06819 [eess.IV]*
- [20] Nelson F Liu, Kevin Lin, John Hewitt, Ashwin Paranjape, Michele Bevilacqua, Fabio Petroni, and Percy Liang. 2024. Lost in the Middle: How Language Models Use Long Contexts. *Transactions of the Association for Computational Linguistics* 11 (2024), 157–173.
- [21] Yue Liu, Yunjie Tian, Yuzhong Zhao, Hongtian Yu, Lingxi Xie, Yaowei Wang, Qixiang Ye, and Yunfan Liu. 2024. VMamba: Visual State Space Model. *ArXiv abs/2401.10166* (2024).
- [22] Meng Lou, Shu Zhang, Hong-Yu Zhou, Chuan Wu, Sibe Yang, and Yizhou Yu. 2025. TransXNet: Learning Both Global and Local Dynamics with a Dual Dynamic Token Mixer for Visual Recognition. *arXiv:2310.19380*
- [23] Anish Mittal, Rajiv Soundararajan, and Alan C. Bovik. 2013. Making a “Completely Blind” Image Quality Analyzer. *IEEE Signal Processing Letters* 20, 3 (2013), 209–212.
- [24] Karen Panetta, Chen Gao, and Sos Agaian. 2016. Human-Visual-System-Inspired Underwater Image Quality Measures. *IEEE Journal of Oceanic Engineering* 41, 3 (2016), 541–551.
- [25] Lintao Peng, Chunli Zhu, and Liheng Bian. 2023. U-Shape Transformer for Underwater Image Enhancement. *IEEE Transactions on Image Processing* 32 (2023), 3066–3079.
- [26] Yan-Tsung Peng and Pamela C. Cosman. 2017. Underwater Image Restoration Based on Image Blurriness and Light Absorption. *IEEE Transactions on Image Processing* 26, 4 (2017), 1579–1594.
- [27] Yuan Shi, Bin Xia, Xiaoyu Jin, Xing Wang, Tianyu Zhao, Xin Xia, Xuefeng Xiao, and Wenming Yang. 2024. Vmambair: Visual state space model for image restoration. *arXiv preprint arXiv:2403.11423* (2024).
- [28] Yi Tang, Hiroshi Kawasaki, and Takafumi Iwaguchi. 2023. Underwater Image Enhancement by Transformer-based Diffusion Model with Non-uniform Sampling for Skip Strategy. *Proceedings of the 31st ACM International Conference on Multimedia* (2023).
- [29] Zhou Wang, A.C. Bovik, H.R. Sheikh, and E.P. Simoncelli. 2004. Image quality assessment: from error visibility to structural similarity. *IEEE Transactions on Image Processing* 13, 4 (2004), 600–612.
- [30] Juan Wen, Weiyan Hou, Luc van Gool, and Radu Timofte. 2025. MatLR: A Hybrid Mamba-Transformer Image Restoration Model. *ArXiv* (2025).
- [31] Zhuofan Xia, Xuran Pan, Shiji Song, Li Erran Li, and Gao Huang. 2022. Vision transformer with deformable attention. In *Proceedings of the IEEE/CVF conference on computer vision and pattern recognition*. 4794–4803.
- [32] Yi Xiao, Qiangqiang Yuan, Kui Jiang, Yuzeng Chen, Qiang Zhang, and Chiao-Wen Lin. 2024. Frequency-Assisted Mamba for Remote Sensing Image Super-Resolution. *ArXiv abs/2405.04964* (2024).
- [33] Xiaohong Yan, Wenqiang Qin, Yafei Wang, Guangyuan Wang, and Xianping Fu. 2022. Attention-guided dynamic multi-branch neural network for underwater image enhancement. *Knowl.-Based Syst.* 258, C (Dec. 2022), 11 pages.
- [34] Brandon Yang, Gabriel Bender, Quoc V Le, and Jiquan Ngiam. 2019. Condeconv: Conditionally parameterized convolutions for efficient inference. *Advances in neural information processing systems* 32 (2019).
- [35] Miao Yang and Arcot Sowmya. 2015. An Underwater Color Image Quality Evaluation Metric. *IEEE Transactions on Image Processing* 24, 12 (2015), 6062–6071.
- [36] Shibai Yin, Shuhao Hu, Yibin Wang, Weixing Wang, Chunxiao Li, and Yee-Hong Yang. 2022. Degradation-aware and color-corrected network for underwater image enhancement. *Knowledge-Based Systems* 258 (2022), 109997.
- [37] Yikang Zhang, Jian Zhang, Qiang Wang, and Zhao Zhong. 2020. Dynet: Dynamic convolution for accelerating convolutional neural networks. *arXiv preprint arXiv:2004.10694* (2020).
- [38] Zou Zhen, Yu Hu, and Zhao Feng. 2024. Freqmamba: Viewing mamba from a frequency perspective for image deraining. *arXiv preprint arXiv:2404.09476* (2024).
- [39] Jingchun Zhou, Jiaming Sun, Chongyi Li, Qiuping Jiang, Man Zhou, Kin-Man Lam, Weishi Zhang, and Xianping Fu. 2024. HCLR-Net: Hybrid Contrastive Learning Regularization with Locally Randomized Perturbation for Underwater Image Enhancement. *Int. J. Comput. Vision* 132, 10 (Feb. 2024), 4132–4156.
- [40] Xizhou Zhu, Weijie Su, Lewei Lu, Bin Li, Xiangang Wang, and Jifeng Dai. 2020. Deformable DETR: Deformable Transformers for End-to-End Object Detection. *ArXiv abs/2010.04159* (2020).